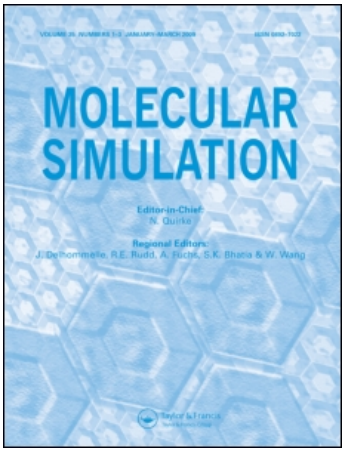

Molecular Simulation
Publication details, including instructions for authors and subscription information:
http://www.informaworld.com/smpp/title~content=t713644482

Molecular studies of the structural properties of hydrogen gas in bulk water

D. Sabo[a]; S. B. Rempe[a]; J. A. Greathouse[b]; M. G. Martin[c]
[a] Computational Bioscience, Sandia National Laboratories, Albuquerque, New Mexico, USA [b] Geochemistry, Sandia National Laboratories, Albuquerque, New Mexico, USA [c] Multiscale Computational Materials Methods, Sandia National Laboratories, Albuquerque, NM, USA

To cite this Article Sabo, D. , Rempe, S. B. , Greathouse, J. A. and Martin, M. G.(2006) 'Molecular studies of the structural properties of hydrogen gas in bulk water', Molecular Simulation, 32: 3, 269 — 278
To link to this Article: DOI: 10.1080/08927020600728621
URL: http://dx.doi.org/10.1080/08927020600728621

Molecular Simulation, Vol. 32, Nos. 3–4, 15 March–April 2006, 269–278

Taylor & Francis
Taylor & Francis Group

Molecular studies of the structural properties of hydrogen gas in bulk water

D. SABO†*, S. B. REMPE†§, J. A. GREATHOUSE‡ and M. G. MARTIN¶

†Computational Bioscience, Sandia National Laboratories, MS 1413 & 0310, Albuquerque, New Mexico 87185, USA
‡Geochemistry, Sandia National Laboratories, MS 0754, Albuquerque, New Mexico 87185, USA
¶Multiscale Computational Materials Methods, Sandia National Laboratories, MS 1110, Albuquerque, NM 87185, USA

(Received March 2006; in final form March 2006)

We report on our studies of the structural properties of a hydrogen molecule dissolved in liquid water. The radial distribution function, coordination number and coordination number distribution are calculated using different representations of the interatomic forces within molecular dynamics (MD), Monte Carlo (MC) and *ab initio* molecular dynamics (AIMD) simulation frameworks. Although structural details differ in the radial distribution functions generated from the different force fields, all approaches agree that the average and most probable number of water molecules occupying the inner hydration sphere around hydrogen is 16. Furthermore, all results exclude the possibility of clathrate-like organization of water molecules around the hydrophobic molecular hydrogen solute.

Keywords: Hydrophobic hydration; Hydrogen; Clathrate hydrate; Coordination number

PACS numbers: 82.20.Wt; 02.60.Pn

1. Introduction

Hydrophobic hydration phenomena are the subject of active research because of their importance in biology and energy technology. In biology, hydrophobic effects play a fundamental role in understanding protein structure, stability and function [1–3]. For example, hydrophobic interactions are considered to be one of the dominant forces driving protein folding as well as formation of micelles and bilayer membranes [4]. In efforts to develop energy technology, hydrophobic interactions are recognized for their role in stabilizing hydrophobic gas particles, such as methane, in solid water structures. Although these solid clathrate hydrates cause difficulties in oil and gas exploration because they tend to clog pipelines [5], the gases stored within these structures also hold potential as a fuel source [6].

While different meanings have been applied to describe the notion of the hydrophobic effect in the literature [2,7], in the context of the present work we refer to the hydrophobic effect as a phenomenon that involves an arrangement of water molecules around a nonpolar solute. On the macroscopic scale, a hydrophobic solute appears to "dislike" water as is, for example, the case in the separation of oil from water. On the microscopic scale involving dissolution of small hydrophobic particles, the presence of a nonpolar solute is associated with disruption of energetically favorable hydrogen bond networks, leading water molecules to "push away" the solute. A more specific structural explanation of the hydrophobic effect has been invoked to explain the observation that dissolution of two hydrophobic Ar gas atoms yields the same change in entropy as dissolution of hydrophilic KCl salt [8]. The structural explanation is that water forms an ordered arrangement around the hydrophobic solute, leading to formation of a local clathrate-like structure [9].

True clathrate structures formed from water and hydrophobic gases exist under specific thermodynamic conditions. These clathrate hydrates belong to a group of inclusion solid-state compounds in which the guest (hydrophobic) molecule occupies the host polyhedra cages that are formed by hydrogen bonded water molecules [10]. A signature of the existence of clathrates comes from the regular numbers of water molecules

*Corresponding author. Email: slrempe@sandia.gov
§Email: dsabo@sandia.gov

Molecular Simulation
ISSN 0892-7022 print/ISSN 1029-0435 online © 2006 Taylor & Francis
http://www.tandf.co.uk/journals
DOI: 10.1080/08927020600728621

forming the host cages, the sequence of possibilities (20, 24, 28, etc.) sometimes referred to as "magic" numbers. One can think of clathrate hydrates as solid solutions of water that trap hydrophobic molecules. Without the presence of the guest molecule(s) and the existence of suitable thermal parameters (temperature and pressure) the clathrate hydrate lattice would be thermodynamically unstable, that is, it would not exist.

Recent experimental results have demonstrated the possibility of synthesizing a whole new class of clathrate hydrates, hydrogen clathrate hydrates [11,12], and raised the prospect of utilizing them as an alternative storage material for hydrogen fuel [13]. The synthesized hydrogen clathrate was found to crystallize by forming the so-called sII type clathrate cubic structure. A unit cell of the sII clathrate consists of 16 "small" (dodecahedral-5^{12}) cages made up of 20 water molecules (see figure 9) and 8 "large" (hexakaidecahedral-$5^{12}6^4$) cages made up of 28 water molecules (see figure 10) [14,15].

The question of what number of hydrogen molecules can be accommodated in the cages of the clathrate is of practical importance because it determines the hydrogen storage capacity of the hydrogen clathrates. Experimental and theoretical studies of the hydrogen occupancy of the hydrogen clathrate cages have been inconclusive on this important issue. Mao *et al.* [12] found that the molecular ratio of H_2 to H_2O was $R = 0.45 \pm 0.05$. Such a value suggests that $2H_2$ molecules occupy the small cages and $4H_2$ molecules occupy the large cages and yields a H_2:H_2O mass ratio of 5.2%. These experimental findings were confirmed by theoretical work of Patchkovskii and Tse [14].

More recently, neutron diffraction studies of the hydrogen clathrate with D_2 guests have reported single and quadruple occupancy of the small and large cages by D_2 molecules, respectively [16]. This cage-occupation arrangement corresponds to H_2:H_2O mass ratio of only 3.9%. It was also shown that the occupation number of the large cages decreases with increasing temperature of the clathrate. Experimental results obtained by neutron diffraction studies were in qualitative agreement, regarding the cage occupancy, with recent molecular dynamics (MD) simulations [17].

Another important consideration involves the conditions under which the clathrates are stable. Hydrogen clathrates were synthesized at relatively harsh conditions: high pressures $\sim$2000 atm and moderately low temperatures $\sim$249 K [12]. It was observed that the hydrogen clathrate preserved its stability at ambient pressure (1 atm) and temperatures lower than 140 K, but at ambient pressure and temperatures of 140 K and higher, the clathrate released the stored hydrogen. In order to be of practical interest for hydrogen storage, the hydrogen clathrates need to be stabilized under more moderate conditions, ideally under standard conditions (1 atm and 298 K). Binary sII clathrate hydrates containing H_2 and THF molecules were synthesized and stabilized at much lower pressure ($\sim$50 atm at 280 K) than the pure hydrogen clathrate ($\sim$2000 atm at 280 K) [18]. The presence of the additive molecule (THF) enables the stabilization of the clathrate at relatively moderate conditions. X-ray diffraction showed that the THF molecules occupy the large cages while the H_2 molecules occupy the small cages. Such a cage-occupation arrangement of the guest molecules, however, diminishes the potential storage capacity of the clathrate.

Recently, Lee *et al.* [19] synthesized binary H_2/THF clathrates at modest pressures by tuning the mole percent (concentration) of THF in the water/H_2 solution. The X-ray diffraction studies of the binary H_2/THF clathrate showed that hydrogen guests occupy small and some large cages while THF guests occupy the remaining large cages. Decreasing the concentration of THF in the solution from 5.6 to 0.15% increases the hydrogen storage capacity from 2.1 to 4.0 wt%. In future work, molecular studies can aid the search for additive molecules that simultaneously maximize hydrogen occupancy and stabilize the clathrate structure at moderate conditions. In addition, molecular studies can confirm the mass ratio of hydrogen occupying both pure clathrates and clathrates with additives.

In the present work, we study the structural properties of hydrogen in liquid water, which are relevant to the clathrate phase as well as to the phenomenon of hydrophobic hydration and the associated hydrophobic effect. Our purpose is to acquire a better microscopic understanding of the water–hydrophobic solute systems, in general, and water–hydrogen systems, in particular. Our goals are to obtain structural information about the size and distribution of water clusters around the hydrogen molecule and to gain insight into trapping of hydrogen by water. In the process, we will address the proposition that local clathrate-like structures stabilize hydrophobic solutes, such as H_2, in liquid water. In addition, we examine the adequacy of and compare different force fields used to model water–water and water–hydrogen interactions to determine which force field could be used as a point of departure for future studies of hydrogen occupancy and hydrogen clathrate hydrate stability.

The remainder of the paper is organized as follows. In Section II we give a brief review of the computational methods and the model potentials employed to calculate the structural properties of water around the hydrogen molecule. In Section III we present the results including the radial distribution functions, hydration numbers and coordination number distributions. Finally, we summarize our findings in Section IV.

2. Computational method

In the present section, we describe the computational details of our studies involving the hydrogen molecule in bulk water. The system is studied by three different computational methods and modeled by three different force fields. MD simulations were performed utilizing the flexible simple point charge (SPC) water model [20,21]

combined with the spherical H_2 model. Monte Carlo (MC) simulations were performed utilizing the extended simple point charge (SPC/E) model potential [22] combined with the 3-site charge H_2 model [17], and *ab initio* molecular dynamics (AIMD) simulations were carried out by calculating forces "on the fly".

2.1 Molecular dynamics simulation

A series of MD simulations were performed to investigate the hydration of H_2 in bulk water. The flexible SPC water model potential [20,21] was used for all simulations. Several H_2–H_2O parameters were used to compare their validity. All H_2 models considered in the present work treat the hydrogen molecule as a single sphere with no atomic charge. A difference between the models lies in the Lennard-Jones parameters. Two models were obtained from studies of hydrogen clathrates [23] assuming single H_2 occupancy in the cages. All potential parameters are listed in table 1, while the potential energy between two monomers, i and j, is given by

$$V_{ij} = \sum_{m\in i}\sum_{n\in j}\frac{q_m q_n}{r_{mn}} + 4\epsilon_{ij}\left[\left(\frac{\sigma_{ij}}{r_{ij}}\right)^{12} - \left(\frac{\sigma_{ij}}{r_{ij}}\right)^{6}\right], \quad (1)$$

where m and n are the charge sites on monomers i and j, respectively, q_m (q_n) is the atomic charge on charge site m associated with monomer i (n associated with monomer j), r_{mn} is the distance between charges on different molecules, r_{ij} is the distance between atomic sites on two monomers and ϵ_{ij} and σ_{ij} are Lennard-Jones parameters. Simple combination rules (Lorentz-Berthelot) [24,25] were used to determine the O^W–H_2 interaction energy (O^W (H^W) denotes the oxygen (hydrogen) atom in the water molecule). Intramolecular degrees of freedom (bond stretch and angle bend) of water molecules were also included in the simulations [20,21].

All MD simulations were performed using the LAMMPS code [26] by employing periodic boundary conditions. Short-range interactions were calculated every 0.5 fs while the long-range portion of the electrostatic interactions were calculated every 1.0 fs by implementing a particle–particle particle-mesh technique [27]. Data were collected during a 1.0-ns production NVE (micro-canonical ensemble) stage, which followed a 0.5-ns equilibration stage. Velocity scaling was used initially with a target temperature of 300 K. Each water box was constructed to give a water density of 1.0 gcm^{-3}. Data were obtained for boxes containing 64, 114 and 215 waters corresponding to box lengths ranging from 12.4 to 18.6 Å. A single H_2 particle was then inserted into each box and new simulations were performed.

Table 1. Potential parameters for the flexible SPC water–H_2 models utilized in the MD simulations.

Atom type	*Description*	*q (e)*	σ_{ij}† (Å)	ϵ_{ij}† (*kcal mol*$^{-1}$)
H_2	Clathrate small cage (5^{12})	0	3.14	0.0190
	Clathrate large cage ($5^{12}6^4$)	0	3.12	0.0188
O^W	Water O	−0.82	3.17	0.155
H^W	Water H	0.41	0	0

†The potential parameters between unlike atoms are determined by simple combination rules (see text).

2.2 Classical Monte Carlo simulation

The properties of interest were computed using the MC for complex chemical systems (MCCCS) Towhee simulation package [28]. Simulations were carried out in the canonical (NVT) ensemble at a temperature of 300 K and the isothermal–isobaric (NpT) ensemble at a temperature of 300 K and a pressure of 1 atm. The simulation box utilized in the NVT ensemble was a cubic box, with sides of length 17 Å and periodic boundary conditions, which contained $1H_2$ molecule surrounded by 136 water molecules. The same number of molecules was used in the NpT ensemble simulations. Simulations were divided into two phases: an equilibration phase that consisted of 400,000 MC cycles (one cycle corresponds to N moves where N is the number of molecules in the system) and an accumulation phase, for which the results are reported, that consisted of 1,000,000 cycles.

The "menu" of the MC moves for the NpT ensemble consist of volume changes, configurational-bias single box molecule reinsertion moves (a move that takes a molecule out of a box and tries to place it back into the same box by growing it using coupled–decoupled configurational-bias (CDCB) MC) [29,30], translation of the center of mass, and rotation about the center of mass. The MC moves for the NVT ensemble consist of translation of the center of mass and rotation about the center of mass of the molecules.

Interactions between molecules in the system were modeled by the SPC/E potential, the functional form given by equation (1). The SPC/E potential treats the water molecules as rigid bodies. Unlike the flexible SPC water potential utilized in the MD simulations, which treats the H_2 molecules as spheres without charge, this potential treats the H_2 molecule as a rigid body with a bond length of 0.7414 Å and a quadrupole moment equal to the experimental gas-phase value [17]. The charges are located on the hydrogen nuclei and at the center of mass of the H_2 molecule (see table 2).

2.3 Ab initio *molecular dynamics simulation*

For all simulations presented here, we utilized the Vienna *ab initio* simulation package (VASP) [31,32] based on a generalized gradient approximation (GGA) of Perdew and Wang (PW91) [33,34] to a plane wave density functional theory with the ultrasoft Vanderbilt pseudopotentials [35,36]. A kinetic energy cut-off of 36.75 Ry defined the

Table 2. Potential parameters for SPC/E water-rigid H_2 molecule model utilized in the MC simulations. These parameters were taken from Ref. [17].

Atom type	*Description*	*q (e)*	σ_{ij}‡ *(Å)*	ϵ_{ij}‡ *(kcal mol^{-1})*
O^W	Water O	−0.8476	3.166	0.1554
H^W	Water H	0.4238	0.000	0.0000
H^A	H in H_2	0.4932	0.000	0.0000
H_2^{CM}	Center of mass of H_2	−0.9864	3.038	0.0682

‡The potential parameters between unlike atoms are determined by simple combination rules (see text).

plane wave basis expansions of the valence electronic wave functions.

The system simulated by AIMD consisted of 1 H_2 molecule and 32 water molecules in a cubic box with sides of length 9.865 Å in periodic boundary conditions. An initial structure of the system was obtained from a previous study of Kr(aq) [7] where the Kr atom was replaced with a hydrogen molecule. All hydrogen atoms in the system were replaced by deuterium atoms.

The system was equilibrated in the NVT ensemble for the first 11.83 ps at a temperature of 300 K and the equations of motion were integrated in time steps of 1 fs. The production phase was carried out in the NVE ensemble for an additional 18.08 ps where a time step of 0.5 fs was used for integrating the equations of motion.

3. Results and discussion

In this section, we present the results of MD, MC and AIMD simulations carried out on the hydrogen molecule solvated in water. Details about the calculations were given in Section II.

3.1. Molecular dynamics

Here we only report the results obtained by simulating the system consisting of one hydrogen and 215 water molecules in the simulation box. Similar results were obtained by simulating the system with 64 and 114 water molecules.

Figure 1 shows an instantaneous number of water molecules that surround the hydrogen molecule within the sphere of radius $r = 4.96$ Å (first hydration shell). The number of water molecules that cluster around the hydrogen molecule varies from 9 to 22.

The hydration shell around H_2 was studied by examining radial distribution functions [25] of O^W–H_2 and H^W–H_2 pairs. The radial distribution functions are shown in figure 2. Both O^W–H_2 and H^W–H_2 radial distribution functions display first maxima at about the same location, around 3.2a Å. This is typical structural behavior for water near a small nonpolar (hydrophobic) solute, that is, it is a well-known feature of hydrophobic

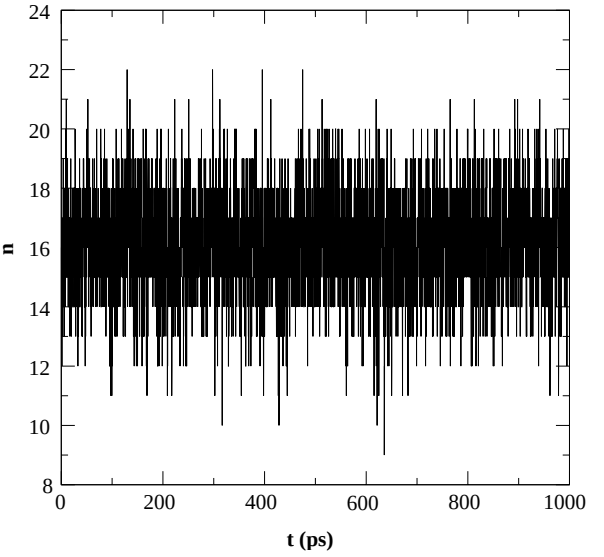

Figure 1. Water coordination number (n) of the hydrogen molecule as a function of time obtained by MD.

hydration (See Ref. [37] and references therein). Although an analysis of the water–water (O^W–O^W) radial distribution function in the system reveals bulk-like structure of water, in the vicinity of a small hydrophobic solute, such as a hydrogen molecule, water molecules are "pushed" further away from the solute and arrange themselves in such a way that their HOH planes lie almost parallel to the solute surface [38]. In other words, water molecules adopt a preferential orientation near a nonpolar solute and they tend to straddle the solute surface [39]. In this way they preserve the most favorable hydrogen-bonding interaction among themselves in which the number of hydrogen bonds is maximized.

A tail in the H^W–H_2 radial distribution function present at the shorter distances (see figure 2, 1.6 Å$\leq r \leq$2.6 Å)

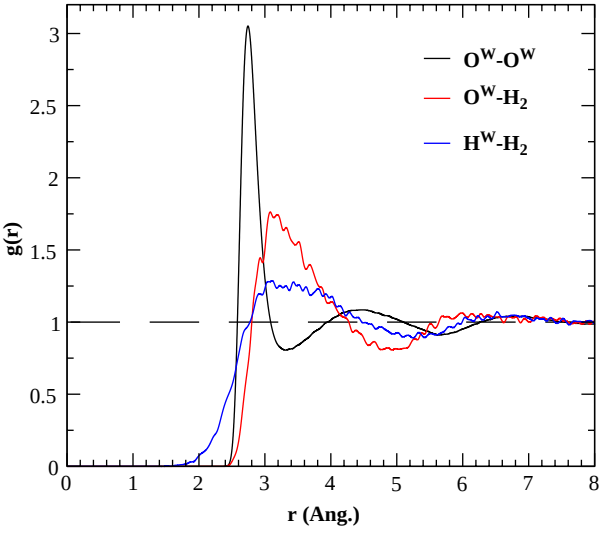

Figure 2. Radial distribution functions obtained by the MD simulation. Water oxygen (O^W)–water oxygen (O^W) (black line), water oxygen (O^W)–hydrogen molecule (H_2) (red line) and water hydrogen (H^W)–hydrogen molecule (H_2) (blue line) radial distribution functions. Radius r is given in units of Å.

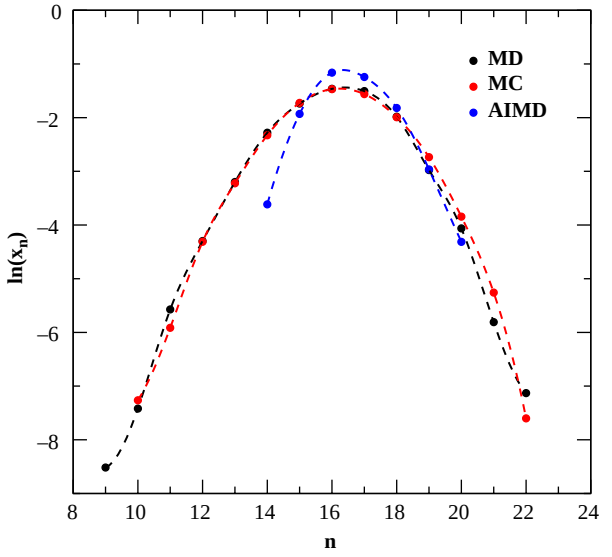

Figure 3. Probability distributions of hydration-shell structures with n water molecules surrounding the H_2 molecule yielded from the MD (black symbols), MC (red symbols) and AIMD (blue symbols) simulations. The hydration-shell boundary is defined at $r = 4.96$ Å for MD and MC simulations while for AIMD simulations it is defined at $r = 4.90$ Å.

indicates that, on average, water hydrogens lie slightly closer to the solute center than water oxygens. This orientation of the water molecules results in the net positive electrostatic potential found at the center of the solute [38].

We estimate another property related to structure, the coordination number $\langle n \rangle$. The coordination number, the average number of water molecules that lie within the radius $r = 4.96$ Å around a solute, was obtained by integrating the O^W–H_2 radial distribution function from zero to the first minimum ($r \in [0, 4.96]$ Å). Integration yielded a numerical value $\langle n \rangle = 16.4$.

A final structural determination of hydrogen hydration was made using cluster statistics. The probability x_n of finding n water molecules within the first hydrogen hydration shell (4.96 Å) was calculated. Snapshots were examined every 0.2 ps. We found that the most probable size of the water cluster surrounding the hydrogen molecule was $n = 16$. This value is consistent with the coordination number estimated above. Figure 3 shows a natural logarithm of the probability that a water cluster of a certain size will enclose the hydrogen molecule. MD results are shown with black symbols and they are in excellent agreement with the MC results (red symbols).

3.2 Monte Carlo

In the current work, we only present the results obtained by simulations carried out in the NpT ensemble. The NVT ensemble simulations yielded similar results.

The instantaneous coordination number n of the hydrogen molecule in liquid water is shown in figure 4. During the simulation the system displays "water cages" around the hydrogen molecule ranging in size from 10 to 22, where 10 and 22 water molecule cages are "visited"

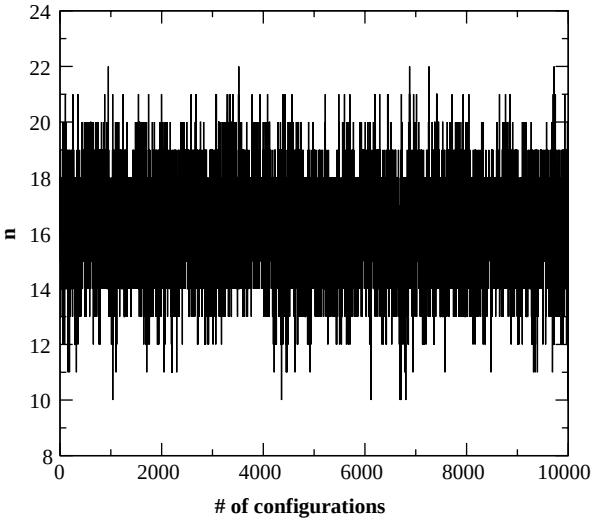

Figure 4. Water coordination number (n) of the hydrogen molecule as a function of the Monte Carlo sampled configurations. Each configuration is recorded after 100 Monte Carlo cycles.

much less frequently than, for example, the cages made up of 16 or 17 water molecules.

An average coordination number $\langle n \rangle = 16.25 \pm 0.29$ was obtained by integrating the O^W–(H_2^{CM}) radial distribution function from zero to the first minimum ($r = 4.96$ Å; see figure 5). The uncertainty in $\langle n \rangle$ was obtained as follows. We carried out two simulations in the NpT ensemble. For each simulation the radial distribution functions were determined by utilizing a different number of bins [25] (75, 100 and 200). Thus, after averaging over six "measurements" we obtained the above listed value for $\langle n \rangle$. The statistical error of 0.29 corresponds to two standard deviations.

After performing cluster statistics, we found $n = 16$ to be the most probable water structure around H_2.

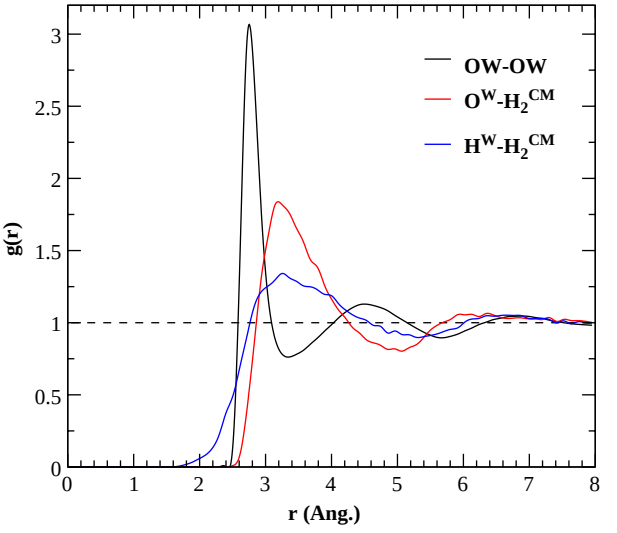

Figure 5. Radial distribution functions obtained by the Monte Carlo method. Water oxygen (O^W)–water oxygen (O^W) (black line), water oxygen (O^W)–center of mass of the hydrogen molecule (H_2^{CM}) (red line) and water hydrogen (H^W)–center of mass of the hydrogen molecule (H_2^{CM}) (blue line) radial distribution functions. Radius r is given in units of Å.

An average most probable coordination number was found as follows. A total number of configurations (10,000) were divided in ten blocks (each block contained 1000 configuration). The most probable coordination number was found for each block and the average most probable coordination number $\langle n_{x_n} \rangle = 16.10 \pm 0.19$ was obtained by averaging over ten blocks. The statistical error corresponds to two standard deviations. The coordination number distribution x_n is shown in figure 3. It can be seen that distributions obtained by MC and MD simulations are in excellent agreement for almost the whole range of cluster sizes. The AIMD distribution agrees well with MD and MC distributions near the mode and its right wing. All three methods yield 16 water molecules as the most probable structural arrangement around the H_2 molecule in liquid water. Although we utilize three different force fields in the simulations, the structural properties of water around the hydrophobic solute turn out to be relatively insensitive to their features.

Complementary structural information about the hydration shell around H_2 was obtained by examining radial distribution functions of O^W–H_2^{CM} and H^W–H_2^{CM} pairs shown in figure 5. When compared to those obtained by MD simulations (see figure 2) one can see that they are almost identical. There are small differences between them, however, that can be seen in figure 6. These differences can be attributed to the nature of the force fields used in the simulations.

A closer look at figure 6 reveals that O^W–H_2^{CM} (black line; obtained by MC) and O^W–H_2^{MD} (blue line; obtained by MD) radial distribution functions are slightly different for short distances, but they agree for larger distances. The hydrogen molecule is modeled as a rigid body with a finite quadrupole moment (3-site charge H_2 model) in the MC simulations while in the MD simulations as a single sphere without charge (spherical H_2 model).

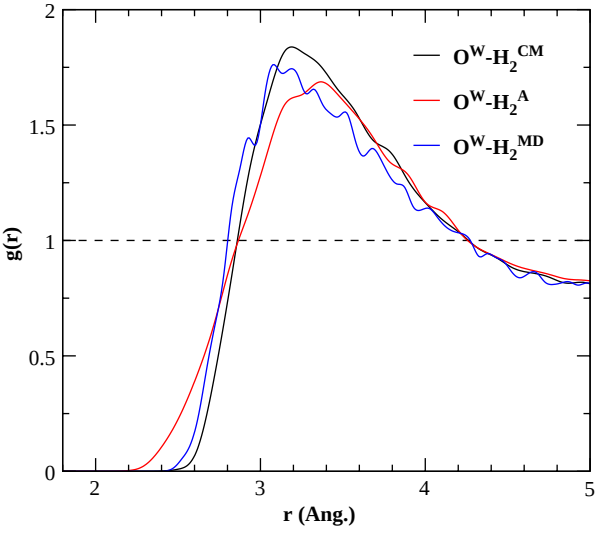

Figure 6. Water oxygen (O^W)–center of mass of the hydrogen molecule (H_2^{CM}) (black line), water oxygen (O^W)–hydrogen atom of the hydrogen molecule (H_2^A) (red line) radial distribution functions obtained by the MC simulation. Water oxygen (O^W)–hydrogen molecule (H_2) (blue line) radial distribution function obtained by the MD simulation. The radial distribution functions are only shown up to the first hydration shell. Radius r is given in units of Å.

At very large distances ($r \geq 4.0$ Å) a water molecule "sees" the hydrogen molecule as a neutral solute (note that the electrostatic potential of a quadrupole moment decreases as $1/r^3$, where r is the distance from the quadrupole moment; see for example Ref. [40]). Thus the reason O^W–H_2^{CM} and O^W–H_2^{MD} radial distribution functions agree at large distances is because hydrogen molecules are seen as neutral species by water molecules in both cases.

At medium separations water molecules begin to "sense" the quadrupole moment on the hydrogen molecule. At shorter separations (2.2 Å $\leq r \leq$ 2.8 Å) a water molecule starts to see individual charges on the hydrogen molecule. On average the oxygen atom from the water molecule (O^W), which carries a negative charge, is more likely to come closer to H_2^{MD} as a neutral species than to H_2^{CM} as a negatively charged species. Thus, at short separations the 3-site model potential for H_2 is slightly more repulsive than the spherical model potential for H_2 which causes the O^W–H_2^{MD} radial distribution function to be shifted to the left of the O^W–H_2^{CM} radial distribution function. The same phenomenon can be seen when we examine the O^W–H_2^A radial distribution function (red line) in figure 6 (H_2^A denotes either one of the hydrogen atoms in the hydrogen molecule). A positively charged hydrogen atom on the hydrogen molecule attracts the negatively charged oxygen atom on the water molecule. On average the oxygen atom ($-q$) comes closer to a hydrogen atom ($+q$) than to the center of mass of the hydrogen molecule ($-q$) and the net result is the large tail in O^W–H_2^A radial distribution function at short separations.

To examine a conventional view [2,41,42] of hydrophobic hydration that the local structure of liquid water around the hydrophobic solute is clathrate-like, we analyzed snapshots that were sampled during the MC simulation. Two representative snapshots displaying a water cluster consisting of 16 and 20 water molecules surrounding the solute are shown in figures 7 and 8, respectively. These figures suggest that water clusters around a hydrophobic solute are cage-like but not clathrate-like in the sense that they do not possess the regular-geometric arrangements of the clathrate phase shown in figures 9 and 10. Furthermore, the coordination number distributions shown in figure 3 indicate that a clathrate-like organization of water clusters around the hydrogen molecule is unlikely to exist. In other words, the magic number water clusters (20, 28—numbers that characterize type II clathrate hydrates) are unlikely to form around the solute in liquid water.

With regard to lack of evidence for clathrate-like structures, our results are consistent with the recent work on the hydration of a krypton atom in liquid water [7,43].

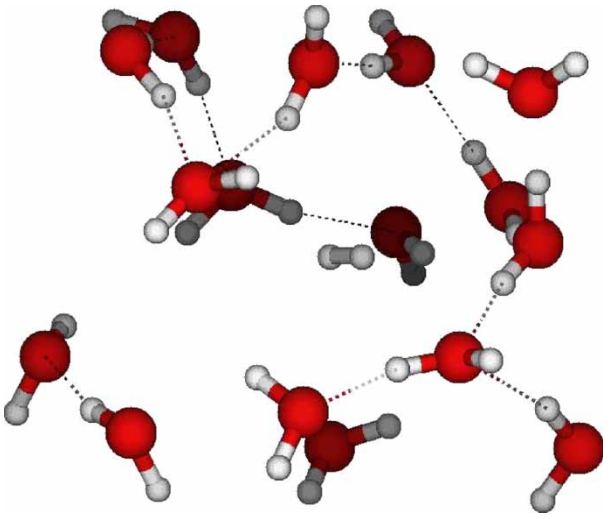

Figure 7. Representative snapshot of the "water cage" structure (made up of 16 water molecules) trapping the hydrogen molecule in liquid water. Hydrogen bonds are depicted by dashed lines. The snapshot was obtained from the Monte Carlo simulation.

3.3 Ab initio *molecular dynamics*

The structural analysis presented here was obtained from an 18.08 ps trajectory generated in the microcanonical ensemble after an equilibration period of 11.83 ps at 300 K carried out in the canonical ensemble.

Figure 11 (upper trace) shows the instantaneous number of water molecules that surround the hydrogen molecule within the sphere of radius $r = 4.9$ Å (first solvation shell). It can be seen that the size of "water clusters" around the solute fluctuates between 14 and 20 water molecules. The lower trace of figure 11 shows the instantaneous temperature of the system. Initially the temperature increased and then settled at 310 ± 7 K. The resulting radial distribution functions are shown in figure 12.

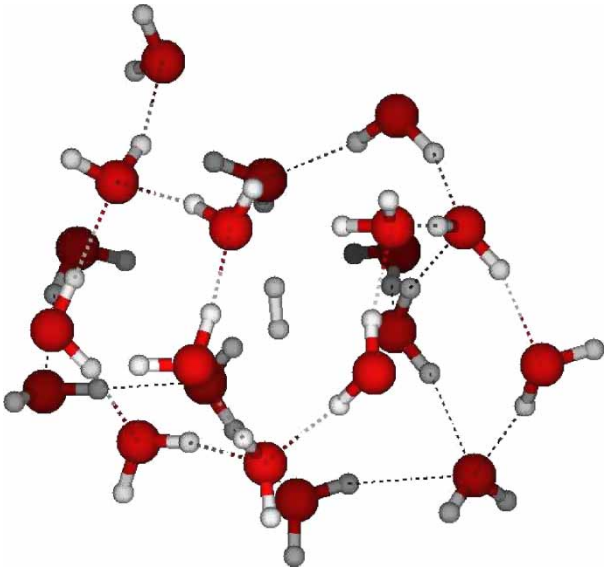

Figure 8. Representative snapshot of the "water cage" structure (made up of 20 water molecules) trapping the hydrogen molecule in liquid water. Hydrogen bonds are depicted by dashed lines. The snapshot was obtained from the Monte Carlo simulation.

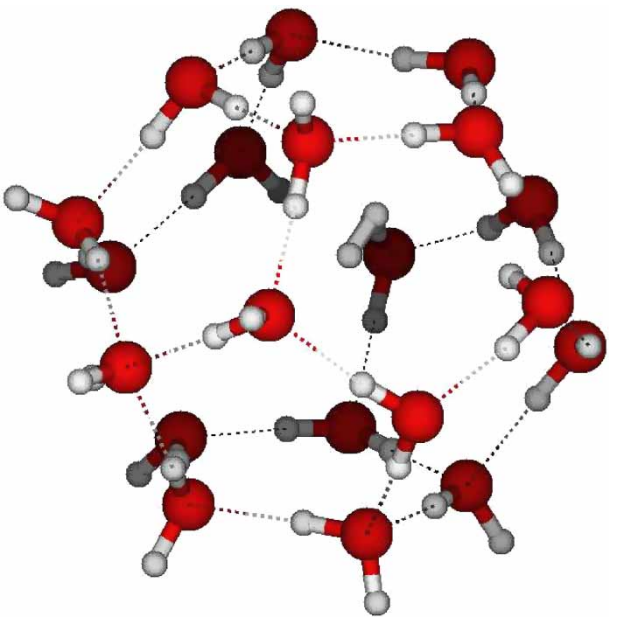

Figure 9. Structure of the small (5^{12}) cage of the type II clathrate hydrate enclosing one hydrogen molecule. The cage consists of 20 water molecules. The notation 5^{12} indicates the number of pentagonal faces (12) making up the polyhedron. Hydrogen bonds are depicted by dashed lines.

When compared to their MD and MC counterparts it can be seen they exhibit the same general characteristics of hydrophobic hydration around small nonpolar solutes, such as bulk-like water structure, water "pushed" away from the solute, and roughly parallel arrangements of water around the hydrophobic solute. More specifically, the classical and AIMD results differ very little at short distances. Small differences appear at larger distances where the AIMD radial distribution functions are more

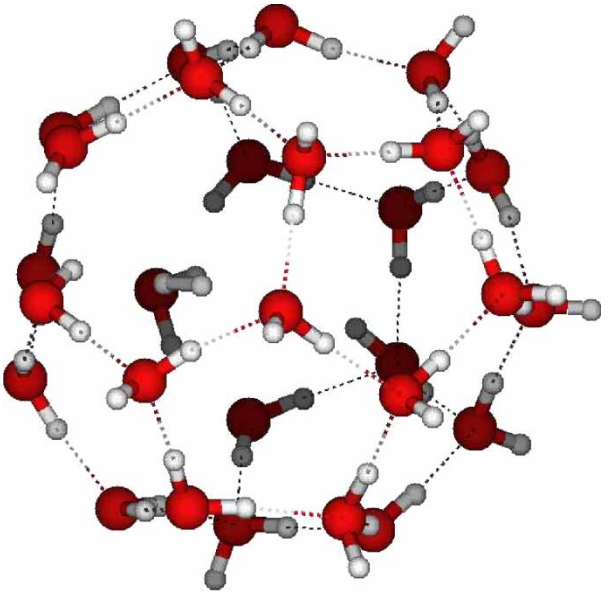

Figure 10. Structure of the large ($5^{12}\ 6^4$) cage of the type II clathrate hydrate enclosing one hydrogen molecule. The cage consists of 28 water molecules. The notation $5^{12}\ 6^4$ indicates the number of pentagonal (12) and hexagonal (4) faces making up the polyhedron. Hydrogen bonds are depicted by dashed lines.

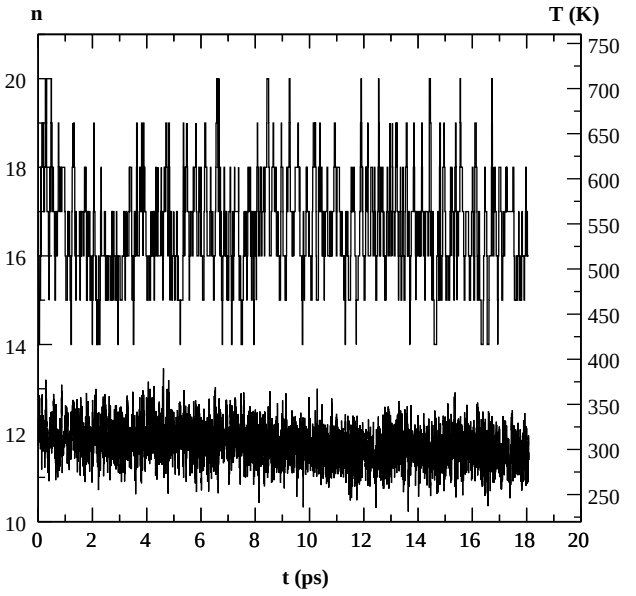

Figure 11. Water coordination number (n) of the hydrogen molecule as a function of time (upper trace and left axis) obtained by AIMD. The lower trace shows the temperature of the system as a function of time.

structured than their MD and MC counterparts. The AIMD distribution functions have a higher peak at the first maximum and a "deeper" first minimum. It has also been observed experimentally that the radial distribution functions for the heavier isotope (D_2) are more structured than for the lighter isotope (H_2) [44]. While the minima and the maxima are located approximately at the same distances as those in the MD and MC radial distribution functions, the maximum of the O^W–H_2^{CM} radial distribution function is slightly shifted toward larger distances ($\approx$3.4 Å) with respect to the MD and MC counterparts, causing a small separation in the positions of water

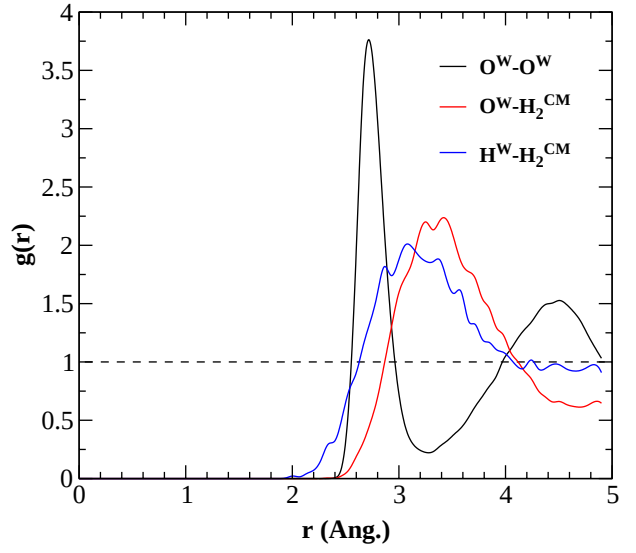

Figure 12. Radial distribution functions obtained by AIMD. Water oxygen (O^W)–water oxygen (O^W) (black line), water oxygen (O^W)–center of mass of the hydrogen molecule (H_2^{CM}) (red line) and water hydrogen (H^W)–center of mass of the hydrogen molecule (H_2^{CM}) (blue line) radial distribution functions. Radius r is given in units of Å.

oxygen and hydrogen atoms and thus tilting of the water molecules away from a planar configuration. Possible reasons for these differences can be identified as:

1. the existence of different charge distributions on the hydrogen molecule and water molecules that lead to more realistic forces in the *ab initio* simulation than those utilized in the classical studies
2. AIMD simulations that have not been run long enough, which is reflected at least in the narrower distribution of structures and larger errors in the wings of the cluster distribution (figure 3), and
3. sensitivity of the results to the density functional used in the AIMD simulations.

Integration of the O^W–H_2^{CM} radial distribution function yields $\langle n \rangle = 16.33$, the same average occupancy of the hydration shell defined by the radius $r = 4.9$ Å as found in the classical studies. Similarly, we find that the most probable water cluster structure around the hydrogen molecule is 16. The average most probable coordination number was obtained by dividing the total number of snapshots (taken every 0.5 ps) into blocks of 1000. For each block the most probable coordination number was found and by averaging over all blocks we obtained the average most probable coordination number $\langle n_{x_n} \rangle = 16.46 \pm 0.24$. The error bar corresponds to two standard deviations. The coordination number distribution is shown in figure 3 by blue symbols.

4. Conclusions

We investigated the structural properties of hydrogen hydration in liquid water by using MD, MC and AIMD with three different force fields: the flexible SPC water model with the spherical H_2 model, the SPC/E water model with the 3-site charge H_2 model and *ab initio* derived forces, respectively.

We find that the most probable water cluster formed around the hydrogen molecule within the first hydration shell contains 16 water molecules. This result is obtained by all three force fields and confirmed by using clustering statistics and by calculating the coordination number distributions (see figure 3).

The radial distribution functions obtained by the spherical H_2 and 3-site charge H_2 models exhibit the first maximum at approximately the same distance ($\approx$3.2 Å) for both oxygen and hydrogen densities. This is a well-known feature of water structure in the vicinity of the hydrophobic solute and implies that the HOH plane of water molecule is oriented almost tangentially to the surface of solute. In other words, the H and O atoms are on average located at the same distance from the solute. At shorter separations (2.2 Å $\leq r \leq$ 2.8 Å) the structural arrangement of water molecules around the hydrogen starts to differ between the two models due to the charge/lack-of-charge distribution on the hydrogen

molecule. The oxygen (hydrogen) density obtained by AIMD is shifted to even longer (shorter) separations with respect to those obtained by the spherical H_2 and 3-site charge H_2 model. These differences may suggest that the classical H_2 models are missing some key components. Accuracy of the two classical force fields models and *ab initio* forces cannot be verified at this point because, to our knowledge, no experimental structural data on aqueous hydrogen is available in the literature.

We note in passing that a conventional view [2,41,42] of hydrophobic hydration, which suggests a local clathrate-like organization of water around the hydrophobic solute, does not hold [7,43]. The coordination number of H_2 in liquid water is 16, a value that differs significantly from the known coordination numbers of true clathrate phases (sI–20, 24 or sII–20, 28). The clathrate-like picture of hydrophobic hydration in the first hydration shell could further be clarified by an in-depth look at the hydrogen bonding within the first hydration shell and the first and second shells. Additional energy [45] and geometric (angle) [46] considerations of hydrogen bonding would also help to distinguish first-shell water molecules from those in the bulk. Since the hydration free energy of hydrogen in liquid water is a well-known thermodynamic quantity [47], calculation of this physical quantity would aid in validating our structural predictions and thus provide additional insight into the hydration of hydrogen in both liquid and clathrate phases. These will be the subjects of future work.

Acknowledgement

The authors would like to thank Randall Cygan and Todd Alam for helpful discussions and critical reading of the manuscript. This work was supported by the LDRD program under Contract DE-AC04-94Al85000. Sandia is a multiprogram laboratory operated by Sandia Corporation, a Lockheed Martin Company, for the US Department of Energy.

References

[1] W. Kauzmann. Some factors in the interpretation of protein denaturation. *Adv. Protein. chem.*, **14**, 1 (1958).
[2] K.A. Dill. Dominant forces in protein folding. *Biochemistry*, **29**, 7133 (1990).
[3] C. Tanford. How protein chemists learned about the hydrophobic factor. *Protein Sci.*, **6**, 1358 (1997).
[4] C. Tanford. Hydrophobic effects and the organization of living matter. *Science*, **200**, 1012 (1978).
[5] I. Chatti, A. Delahaye, L. Fournaison, J.-P. Petitet. Benefits and drawbacks of clathrate hydrates: a review of their areas of interest. *Energy Convers. Manage.*, **46**, 1333 (2005).
[6] E. Suess, G. Bohrmann, J. Greinert, E. Lausch. Flammable ice. *Sci. Am.*, **281**, 76 (1999).
[7] H.S. Ashbuagh, D. Asthagiri, L.R. Pratt, S.B. Rempe. Hydration of krypton and consideration of clathrate models of hydrophobic effects from the perspective of quasi-chemical theory. *Biophys. Chem.*, **105**, 323 (2003).
[8] H.L. Friedman, C.V. Krishnan. In *Water: A Comprehensive Treaties*, F. Franks (Ed.), Vol. 3, p.1, Plenum Press, New York (1998).
[9] H.S. Frank, M.W. Evans. Free volume and entropy in condensed systems. III. Entropy in binary liquid mixtures; partial molal entropy in dilute solutions; structure and thermodynamics in aqueous electrolytes. *J. Chem. Phys.*, **13**, 507 (1945).
[10] E.D. Sloan. *Clathrate Hydrates of Natural Gases*, Marcel Dekker Inc., New York (1998).
[11] Y.A. Dyadin, E.D. Larinov, A.Y. Manakov, F.V. Zhurko, E.Y. Aladko, T.V. Mikina, V.Y. Komarov. Clathrate hydrates of hydrogen and neon. *Mendeleev Commun.*, **5**, 209 (1999).
[12] W.L. Mao, H.-K. Mao, A.F. Goncharov, V.V. Struzhkin, Q. Guo, J. Hu, J. Shu, R.J. Hemley, M. Somayazulu, Y. Zhao. Hydrogen clusters in clathrate hydrate. *Science*, **297**, 2247 (2002).
[13] W.L. Mao, H.-K. Mao. Hydrogen storage in molecular compounds. *Proc. Natl. Acad. Sci. U.S.A.*, **101**, 708 (2004).
[14] S. Patchkovskii, J.S. Tse. Thermodynamic stability of hydrogen clathrates. *Proc. Natl. Acad. Sci. U.S.A.*, **100**, 14645 (2003).
[15] B.C. Chakoumakos, C.J. Rawn, A.J. Rondinone, L.A. Stern, S. Circone, S.H. Kirby, Y. Ishii, C.Y. Jones, B.H. Toby. Temperature dependence of polyhedral cage volumes in clathrate hydrates. *Can. J. Phys.*, **81**, 183 (2003).
[16] K.A. Lokshin, Y. Zhao, D. He, W.L. Mao, H.-K. Mao, R.J. Hemley, M.V. Lobanov, M. Greenblatt. Structure and dynamics of hydrogen molecules in the novel clathrate hydrate by high pressure neutron diffraction. *Phys. Rev. Lett.*, **93**, 125503 (2004).
[17] S. Alavi, J.A. Ripmeester, D.D. Klug. Molecular-dynamics study of strucuture II hydrogen clathrates. *J. Chem. Phys.*, **123**, 024507 (2005).
[18] L.J. Florusse, C.J. Peters, J. Schoonman, K.C. Hester, C.A. Koh, S.F. Dec, K.N. Marsh, E.D. Sloan. Stable low-pressure hydrogen clusters stored in a binary clathrate hydrate. *Science*, **306**, 469 (2004).
[19] H. Lee, J.-W. Lee, D.Y. Kim, J. Park, Y.-T. Seo, H. Zeng, I.L. Moudrakovski, C. I. Ratcliffe, J.A. Ripmeester. Tuning clathrate hydrates for hydrogen storage. *Nature*, **434**, 743 (2005).
[20] O. Teleman, B. Jönsson, S. Engström. A molecular dynamics simulation of a water model with intramolecular degrees of freedom. *Mol. Phys.*, **60**, 193 (1987).
[21] T.I. Mizan, P.E. Savage, R.M. Ziff. Molecular dynamics of supercritical water using a flexible SPC model. *J. Phys. Chem.*, **98**, 13067 (1994).
[22] H.J.C. Berendsen, J.R. Grigera, T.P. Straatsma. The missing term in effective pair potentials. *J. Phys. Chem.*, **91**, 6269 (1987).
[23] J.B. Klauda, S.I. Sandler. Phase behavior of clathrate hydrates: a model for single and multiple gas component hydrates. *Chem. Eng. Sci.*, **58**, 27 (2003).
[24] J.O. Hirschfelder, C.F. Curtiss, R.B. Bird. *Molecular Theory of Gases and Liquids*, p. 168, Wiley, New York (1954).
[25] M.P. Allen, D.J. Tildesley. *Computer Simulation of Liquids*, Oxford University Press, Oxford (1996).
[26] S.J. Plimpton. Fast parallel algorithms for short-range molecular dynamics. *J. Comp. Phys.*, **117**, 1 (1995).
[27] S.J. Plimpton, R.D. Pollock, M.J. Stevens. Particle-mesh Ewald and rRESPA for parallel molecular dynamics simulations, *8th SIAM Conference on Parallel Processing for Scientific Computing*, Minneapolis, MN, USA (1997).
[28] Available online at: http://towhee.sourceforge.net.
[29] M.G. Martin, J.I. Siepmann. Novel configurational-bias Monte Carlo method for branched molecules. Transferable potentials for phase equilibria. 2. United-atom description of branched alkanes. *J. Phys. Chem. B*, **103**, 4508 (1999).
[30] D. Frenkel, B. Smit. *Understanding Molecular Simulation*, Academic Press, San Diego (2002).
[31] G. Kresse, J. Hafner. *Ab initio* molecular dynamics for liquid metals. *Phys. Rev. B*, **47**, RC558 (1993).
[32] G. Kresse, J. Furthmüller. Efficient iterative schemes for *ab initio* total-energy calculations using a plane-wave basis set, *Phys. Rev. B*, **54**, 11169 (1996).
[33] Y. Wang, J.P. Perdew. Correlation hole of the spin-polarized electron gas with exact small-wave-vector and high-density scaling. *Phys. Rev. B*, **44**, 13298 (1991).
[34] J.P. Perdew, J.A. Chevary, S.H. Vosko, K.A. Jackson, M.R. Pederson, D.J. Singh, C. Fiolhais. Atoms, molecules, solids, and surfaces: Applications of the generalized gradient approximation for exchange and correlation. *Phys, Rev B*, **46**, 6671 (1992).
[35] D. Vanderbilt. Soft self-consistent pseudopotentials in a generalized eigenvalue formalism. *Phys. Rev. B*, **41**, 7892 (1990).

[36] G. Kresse, J. Hafner. Norm-conserving and ultrasoft pseudopotentials for first-row and transition-elements, *J. Phys. Condens. Matter*, **6**, 8245 (1994).
[37] L.R. Pratt. Molecular theory of hydrophobic effects: "She is too mean to have her name repeated". *Annu. Rev. Phys. Chem.*, **53**, 409 (2002).
[38] S. Rajamani, T. Ghosh, S. Garde. Size dependent ion hydration, its asymmetry, and convergence to macroscopic behavior. *J. Chem. Phys.*, **120**, 4457 (2004).
[39] F.H. Stillinger. Water revisited. *Science*, **209**, 451 (1980).
[40] J.D. Jackson. *Classical Electrodynamics*, John Wiley & Sons, New York (1975).
[41] Y. Cheng, P.J. Rossky. Surface topography dependence of biomolecular hydrophobic hydration. *Nature*, **392**, 696 (1998).
[42] D.N. Glew. Aqueous solubility and the gas-hydrates, The methane-water system. *J. Chem. Phys.*, **66**, 605 (1962).
[43] R.A. LaViolette, K.L. Copeland, L.R. Pratt. Cages of water coordinating Kr in aqueous solution. *J. Phys. Chem. A*, **107**, 11267 (2003).
[44] J. Urquidi. Private communnication.
[45] A.G. Kalinichev, Y.E. Gorbaty, A.V. Okhulkov. Structure and hydrogen bonding of liquid water at high hydrostatic pressures: Monte Carlo NpT-ensemble simulations up 10 kbar. *J. Mol. Liq.*, **82**, 57 (1999).
[46] T.M. Raschke, M. Levitt. Nonpolar solutes enhance water structure within hydration shells while reducing interactions between them. *Proc. Natl. Acad. Sci. U.S.A.*, **102**, 6777 (2005).
[47] C.L. Young (Ed.). *Hydrogen and Deuterium (Solubility data series)*, Vol. 5/6, Pergamon Press, Oxford (1981).